Published in final edited form as:
Cell Metab. 2016 February 09; 23(2): 265–79. doi:10.1016/j.cmet.2016.01.002.

HIF-1α Promotes Glutamine-Mediated Redox Homeostasis and Glycogen-Dependent Bioenergetics to Support Post-Implantation Cell Survival

Steve Stegen[a,b], **Nick van Gastel**[a,b], **Guy Eelen**[c], **Bart Ghesquière**[c], **Flora D'Anna**[d], **Bernard Thienpont**[d], **Jermaine Goveia**[c], **Sophie Torrekens**[a], **Riet Van Looveren**[a], **Frank P. Luyten**[b,e], **Patrick H. Maxwell**[f], **Ben Wielockx**[g], **Diether Lambrechts**[d], **Sarah-Maria Fendt**[#h], **Peter Carmeliet**[#c], **Geert Carmeliet**[a,b]

[a]Laboratory of Clinical and Experimental Endocrinology, Department of Clinical and Experimental Medicine, KU Leuven, 3000 Leuven, Belgium

[b]Prometheus, Division of Skeletal Tissue Engineering, KU Leuven, 3000 Leuven, Belgium

[c]Laboratory of Angiogenesis & Vascular Metabolism, Vesalius Research Center, Department of Oncology, KU Leuven/VIB, 3000 Leuven, Belgium

[d]Laboratory of Translational Genetics, Vesalius Research Center, Department of Oncology, KU Leuven/VIB, 3000 Leuven, Belgium

[e]Skeletal Biology and Engineering Research Center, Department of Development and Regeneration, KU Leuven, 3000 Leuven, Belgium

[f]Cambridge Institute for Medical Research, University of Cambridge Cambridge CB2 0XU, UK

[g]Heisenberg Research group, Department of Clinical Pathobiochemistry, Institute for Clinical Chemistry and Laboratory Medicine, Technische Universität Dresden, Dresden, Germany

[h]Laboratory of Cellular Metabolism and Metabolic Regulation, Vesalius Research Center, Department of Oncology/VIB, KU Leuven, 3000 Leuven, Belgium

[#] These authors contributed equally to this work.

Summary

Cell-based therapy is a promising strategy in regenerative medicine, but the poor survival rate of the implanted cells remains a major challenge and limits clinical translation. We preconditioned periosteal cells to the hypoxic and ischemic environment of the bone defect site by deleting prolyl hydroxylase domain-containing protein 2 (PHD2), resulting in hypoxia-inducible factor-1 alpha (HIF-1α) stabilization. This strategy increased post-implantation cell survival and improved bone

Correspondence to: Geert Carmeliet.

Corresponding Author: Geert Carmeliet, M.D., Ph.D., Laboratory of Clinical and Experimental Endocrinology, Department of Clinical and Experimental Medicine, KU Leuven, O&N1 Herestraat 49 bus 902, 3000 Leuven, Belgium, Tel.: 0032 16 330 731, Fax: 0032 16 330 718. geert.carmeliet@med.kuleuven.be.

Author Contributions:
S.S., N.v.G., D.L., S.-M.F., P.C. and G.C. designed research, S.S., N.v.G., G.E., B.G., F.D'A., B.T., J.G., S.T., and R.v.L. performed research, P.H.M., B.W. and P.C. contributed new reagents, S.S., N.v.G., G.E., B.G., S.-M.F. and G.C. analyzed data; and S.S. and G.C. wrote the manuscript.

Europe PMC Funders Author Manuscripts

regeneration. The enhanced cell viability was angiogenesis-independent, but relied on combined changes in glutamine and glycogen metabolism. HIF-1α stabilization stimulated glutaminase-mediated glutathione synthesis, maintaining redox homeostasis at baseline and during oxidative or nutrient stress. Simultaneously, HIF-1α signaling increased glycogen storage, preventing an energy deficit during nutrient or oxygen deprivation. Pharmacological inhibition of PHD2 recapitulated the adaptations in glutamine and glycogen metabolism and consequently the beneficial effects on cell survival. Thus, targeting cellular metabolism is an appealing strategy for bone regeneration and cell-based therapy in general.

Abstract

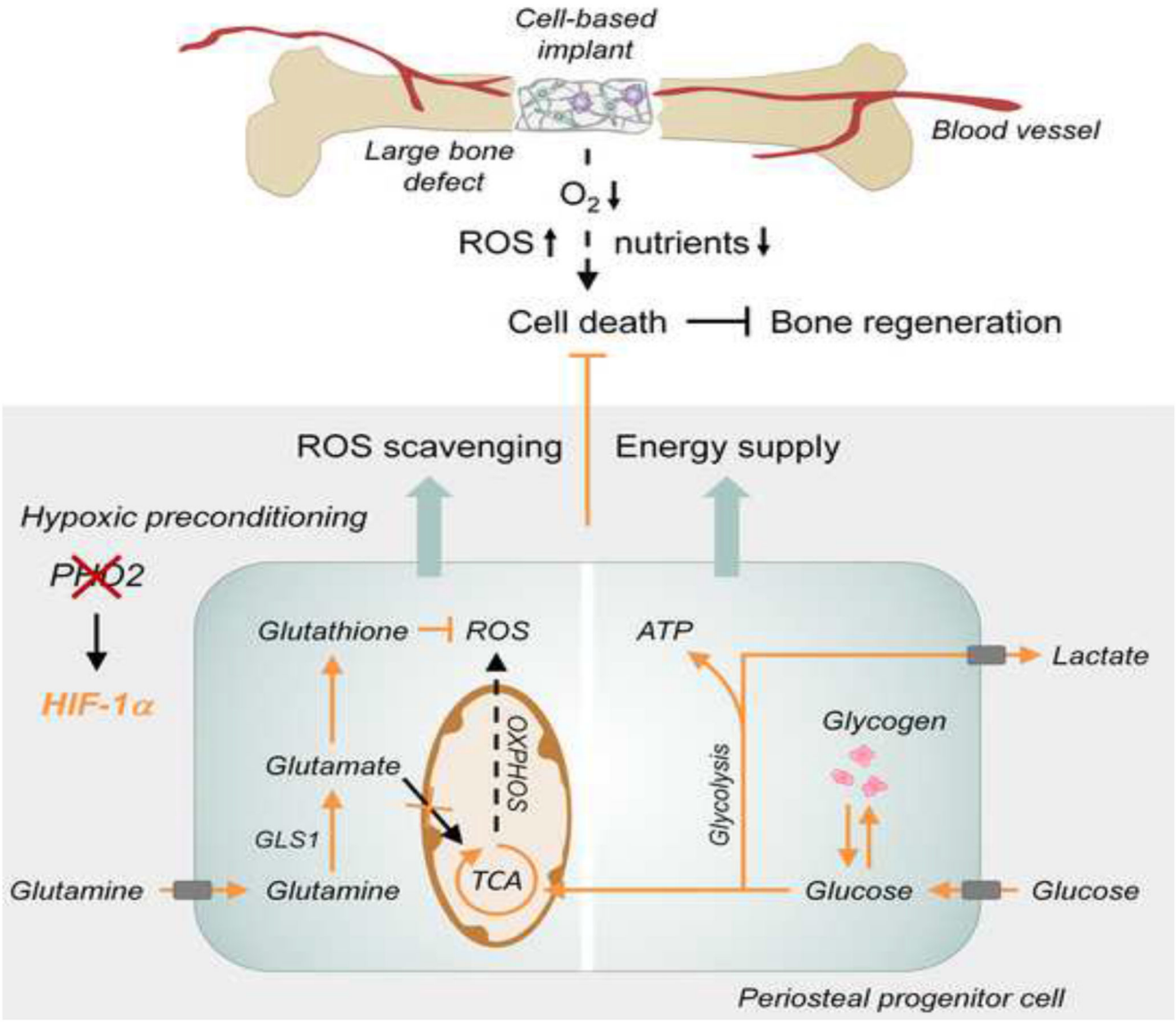

Graphical Abstract.

Europe PMC Funders Author Manuscripts

Introduction

Recent developments in regenerative medicine, using transplantation of stem or progenitor cells, are promising. However, cell-based engineering of large defects remains a major challenge as only 10 to maximally 60% of the implanted cells survive in models of myocardial infarction (Hansson et al., 2009), stroke (Rosado-de-Castro et al., 2013), pancreatic islet transplantation (Zheng et al., 2012) or bone regeneration (Muschler et al., 2004). The massive cell death can largely be explained by the compromised supply of oxygen and nutrients to the transplantation site (Jain et al., 2005; Rouwkema et al., 2008). Vascular ingrowth alleviates this stressful condition (Stegen et al., 2015), but angiogenesis is limited to less than 1 millimeter per day and is thus insufficient to timely revascularize large tissue defects (Laschke et al., 2006).

To improve the success of cell therapy, strategies have been developed to precondition the cells *ex vivo* to a hostile environment, and thereby promote their *in vivo* survival and functional performance. Indeed, the administration of cells exposed to hypoxic preconditioning improves brain, heart or muscle function in preclinical ischemic disease models (Francis and Wei, 2010; Kim et al., 2009; Liu et al., 2012). This beneficial outcome has been attributed to altered behavior of the implanted cells, including secretion of factors that promote neovascularization and recruitment of host cells. In addition, autocrine signaling of cytokines and growth factors may contribute to the survival of the implanted cells (Muscari et al., 2013). On the other hand, recent studies in tumor cells indicate that besides enhanced growth factor signaling (Hanahan and Weinberg, 2011), cancer cells rely on adaptations in cellular metabolism to survive in hypoxic and nutrient-deprived conditions (Semenza, 2013). In these hypoxic tumor cells the activity of the hypoxia-inducible factor (HIF), a critical transcription factor in hypoxia signaling, is often increased and adjusts oxygen and nutrient metabolism to preserve energy and redox balance (Aragones et al., 2009; DeBerardinis et al., 2008). Yet, metabolic adaptations in response to hypoxic preconditioning are hardly studied in cell transplantation strategies, although understanding whether and how preconditioned cells adjust bioenergetics and/or redox homeostasis to survive oxygen and nutrient deprivation is crucial to improve therapeutic strategies.

Similar to the development in other fields of regenerative medicine, cell-based therapies are intensively being studied for skeletal repair and face the same problem of low survival rate (Grayson et al., 2015). In contrast to other regenerative fields, the beneficial effect of hypoxic preconditioning of cells for bone regeneration is unexplored. Yet, hypoxia signaling is known to contribute to bone formation during development and repair and is primarily attributed to increased vascularization. Indeed, non-specific pharmacological inhibition of prolyl hydroxylase domain proteins (PHDs) stabilizes HIF-1α proteins and improves repair of small bone defects (Wan et al., 2008; Shen et al., 2009). During bone growth, increased HIF-1α activity in osteoprogenitor cells enhances bone formation by promoting osteoblast differentiation (Regan et al., 2014). However, the HIF-regulated processes involved in bone development, like vascular ingrowth and osteoblast differentiation, require several days to occur and can thus not explain the improved cell survival observed during the first days after implantation when implanted cells were hypoxic preconditioned.

In the present study we question whether and how hypoxic preconditioning of skeletal cells affects bone regeneration. We demonstrate that inactivation of PHD2 in skeletal cells prior to implantation, increases HIF-1α signaling and improves cell survival, not by enhancing angiogenesis, but by adapting glutamine and glucose metabolism. The combination of these metabolic changes is required to preserve redox and energy balance. Redox homeostasis is maintained by glutaminase (GLS1)-mediated glutathione synthesis whereas energy balance is sustained by increased glycogen storage, demonstrating that targeting skeletal cell metabolism represents a therapeutic target for bone regeneration and regenerative medicine.

Results

Inactivation of PHD2 Improves Cell Survival and Enhances Bone Regeneration

We used a validated model for bone regeneration to investigate the *in vivo* survival rate of implanted osteogenic cells. Murine periosteum-derived cells (mPDC), an established source of skeletal progenitor cells (van Gastel et al., 2012), were seeded onto a calcium phosphatecollagen scaffold and implanted subcutaneously in nude mice. Three days after implantation, most of the cells were undergoing apoptosis, as shown by TUNEL staining on histological sections and Annexin V-PI (AnxV-PI) flow cytometry analysis on implanted CM-FDA labeled cells (Figures 1A,B). Cell apoptosis was most prominent in the center (Figure 1A) and was associated with hypoxia and ROS-induced oxidative DNA damage, shown on histological sections by hypoxyprobe and 8-OHdG staining, respectively (Figure 1C). Staining for the endothelial marker CD31 revealed an angiogenic response at the periphery, but the blood vessels did not yet invade the scaffold (Figure S1A), resulting in compromised oxygen and likely also nutrient supply especially in the center.

To explore whether increased HIF signaling improved cell survival, we deleted PHD2, the most highly expressed isoform in mPDC (Figure S1B). Transduction of *Phd2*$^{fl/fl}$ mPDC with adenovirus-Cre resulted in a marked reduction of PHD2 protein levels (PHD2^{KD}), leading to stabilization of HIF-1α, but not HIF-2α, in normoxia (Figures 1D and S1C). In addition, *Phd3*, but not *Phd1*, gene expression was compensatory increased but not to the level of *Phd2* in control cells (Figure S1B). PHD2 silencing significantly improved cell survival at day three after implantation, evidenced by fewer TUNEL^{+}-stained cells on histological sections (Figures 1E,F) and more viable CM-FDA^{+}AnxV^{-}PI^{-} PHD2^{KD} mPDC by flow cytometry analysis (Figure 1G). Centrally localized PHD2^{KD} cells were better adapted to the hypoxic environment, possibly through decreased oxygen consumption, and showed reduced ROS-induced DNA damage (Figure 1H). The beneficial effect on cell survival could not be explained by enhanced vascular ingrowth (Figure S1D), although PHD2-silenced cells secreted more vascular endothelial growth factor and placental growth factor *in vitro*, which increased endothelial cell survival and network formation (Figures S1E-G). Likely, the slow rate of vascular ingrowth may explain why the scaffolds are still devoid of blood vessels in this early phase despite increased angiogenic growth factor production.

To test whether the increased survival of PHD2^{KD} cells improved their regenerative potential, we quantified the newly formed bone in the scaffolds eight weeks after implantation. Histomorphometry of H&E-stained sections revealed that PHD2^{KD} cells stimulated bone formation throughout the scaffold (Figure 1I), while control mPDC-seeded

scaffolds contained bone only at the periphery and were filled with fibrous tissue in the central regions. At this later time point, the higher bone mass in the PHD2^{KD} mPDC-seeded scaffolds was associated with an increase in blood vessel size and number (Figure S1H). To prove the clinical relevance, we implanted mPDC-seeded scaffolds in a mid-diaphyseal segmental bone defect, which does not heal spontaneously when left empty (van Gastel et al., 2014). In analogy with the ectopic model, silencing PHD2 markedly improved cell survival at day three after implantation (Figures S2A,B), which was associated with a reduced number of hypoxyprobe^{+} and 8-OHdG^{+} cells (Figure S2B). Again, the beneficial effect of PHD2 silencing on cell survival was not related to changes in blood vessel ingrowth (Figures S2C,D). Eight weeks after implantation, significantly more bone was formed in the PHD2^{KD} mPDC-seeded scaffolds, and the difference with control cells was again most prominent in the center, evidenced by micro-computed tomography and histomorphometry (Figures S2E,F).

Together, these data show that PHD2 silencing improves bone regeneration by enhancing the survival of the implanted cells. PHD2^{KD} cells did not alter blood vessel ingrowth at this early stage, suggesting that metabolic adaptations are important for survival.

Silencing PHD2 Enhances ROS Detoxification

Cell survival in stress conditions, like hypoxia, depends on controlling redox balance and avoiding the toxic effects of reactive oxygen species (ROS). Cellular respiration is a major source of ROS, which are neutralized by several scavenging systems. PHD2 inactivation resulted in a reduced oxygen consumption rate (OCR) (Figure 2A) and increased transcript levels of the scavenging proteins superoxide dismutase 1 (SOD1), SOD2 and catalase (Figure S3A). Moreover, PHD2^{KD} cells showed a manifest increase in the total levels of the antioxidant glutathione (Figure S3B) and in the ratio of reduced glutathione (GSH) to oxidized glutathione (GSSG) (Figure 2B). The increase in glutathione peroxidase 1 and glutathione reductase mRNA levels may additionally point to an increased conversion rate from oxidized to reduced glutathione (Figure S3C). In total, these adaptations resulted in decreased mitochondrial and total intracellular ROS levels (Figures 2C,D). To evaluate the biological relevance of these changes, we examined the ability of PHD2^{KD} cells to survive during oxidative stress by adding exogenous ROS or by hypoxia exposure which increases complex III-dependent superoxide generation (Guzy et al., 2005; Waypa et al., 2010). Upon treatment with hydrogen peroxide (H_2O_2) or culture in 0.5% oxygen, the increase in total intracellular ROS levels was less pronounced in PHD2^{KD} cells compared to control cells (Figures 2E,F) and their survival rate was better preserved in these stress conditions (Figures 2G,H).

Thus, PHD2 silencing prevents excessive ROS accumulation in stress conditions, resulting in improved cell survival.

Increased Glutamine-Derived Glutathione Production Is Necessary for Survival of PHD2^{KD} mPDC During Oxidative Stress

Since total glutathione levels were elevated in PHD2^{KD} cells, we questioned whether glutathione synthesis was altered in these cells. Gene expression levels of γ-

glutamylcysteine synthetase and glutathione synthetase were however not affected by PHD2 silencing (Figure S4A), suggesting that the supply of metabolite substrates for glutathione synthesis may be altered.

Glutamine is an important precursor for glutathione, after being converted into glutamate by glutaminase (GLS). PHD2-silenced cells displayed a 3-fold increase in glutamine uptake from the culture medium (Figure 3A) and showed increased expression of GLS1, the most abundant isoform in mPDC, but not of GLS2 (Figures 3B and S4B,C). No change was noticed in mRNA levels of glutamate dehydrogenase, which can alter the fate of glutamate by converting it into α-ketoglutarate (α-KG) (Figure S4C). Next, we investigated the direct contribution of glutamine to glutamate and glutathione using $^{13}C_5$-glutamine as a tracer, and found that silencing of PHD2 increased the fractional contribution from $^{13}C_5$-glutamine to glutamate by 57% and to glutathione by 51% compared to control cells (Figures 3C,D). In contrast, fractional contribution from $^{13}C_5$-glutamine in the tricarboxylic acid (TCA) cycle intermediates fumarate, malate and citrate was decreased in PHD2^{KD} cells (Figure S4D), suggesting that glutamine was not used as a carbon source for TCA anaplerosis, but that glutamine was rather utilized for glutathione production. Of note, the higher fractional contribution from $^{13}C_5$-glutamine in α-KG was caused by the high exchange flux with glutamate (Buescher et al., 2015).

To determine the biological role of GLS1 in maintaining redox homeostasis in PHD2^{KD} cells, we assessed the effect of genetic or pharmacological interference with GLS1 on glutathione-mediated ROS detoxification. Silencing of GLS1 by shRNA (PHD2^{KD}GLS1^{KD}; Figures S4E,F) reduced the GSH:GSSG ratio in control and PHD2^{KD} cells to comparable low levels (Figure 3E). This resulted in elevated ROS levels (Figure 3F) and completely abrogated the pro-survival effect of PHD2 silencing during oxidative stress (Figure 3G). Notably, silencing of GLS2 did not alter ROS levels (Figure S4G). In agreement with the GLS1 silencing data, treatment with the specific GLS1 inhibitor bis-2-(5-phenylacetamido-1,3,4-thiadiazol-2-yl)ethyl sulfide (BPTES) decreased the GSH:GSSG ratio in control and mutant cells, causing an increase in ROS levels and a marked reduction in the survival of PHD2^{KD} cells after H_2O_2 exposure (Figures S4H-J). Importantly, the addition of glutamate, but not of the TCA cycle intermediates (dimethyl) α-KG, citrate, malate or oxaloacetate rescued the viability of H_2O_2-exposed, BPTES-treated PHD2^{KD} or control cells (Figures 3H and S4K). These data indicate that during oxidative stress PHD2^{KD} cells rely on GLS1 for maintaining redox balance, rather than for resupplying the TCA cycle. To determine the *in vivo* importance of enhanced GLS1 action in the pro-survival effect of PHD2 knockdown (Figure 1F), we implanted PHD2^{KD}GLS1^{KD} cells ectopically and observed that GLS1 silencing significantly increased the number of apoptotic PHD2^{KD} cells, hereby mirroring the *in vitro* results (Figure 3I). In addition, silencing GLS1 in wild-type cells decreased their low cell viability *in vivo* even more, emphasizing the role of glutamine metabolism in supporting cell survival in deprived conditions (Figure S4L).

We next examined whether elevated GLS1 levels would be sufficient to maintain redox balance and cell survival in stress conditions. To this end, we transduced periosteal cells with a lentivirus encoding human GLS1 (hGLS1^{OE}), which shows 93% homology with murine GLS1, resulting in increased expression of hGLS1 at the mRNA and protein level (Figures

S4M,N). Ectopic overexpression of hGLS1 largely mimicked the effects observed in PHD2^{KD} cells, as these hGLS1^{OE} cells were more resistant to H_2O_2-induced oxidative damage compared to control cells (Figure 3J). In addition, hGLS1^{OE} cells showed an increase in glutamine uptake rate (Figure S4O), $^{13}C_5$-glutamine contribution to glutathione (Figure 3K) and GSH:GSSG ratio (Figure 3L), as well as dampened basal and H_2O_2-induced intracellular ROS production (Figure 3M). Of note, the fact that hGLS1 overexpression did not fully copy the effects of PHD2 silencing is possibly due to lower enzyme activity.

Thus, the pro-survival effect of PHD2 silencing depends on increased protection to oxidative stress mediated by enhanced conversion of glutamine into glutathione, controlled by GLS1.

PHD2^{KD} Cells Reduce Cellular Respiration but Maintain Their Energy State

Cell survival in stress conditions not only depends on redox balance but also on energy status, which often requires reprogramming of energy metabolism. PHD2^{KD} cells displayed an increase in glucose uptake (Figures S5A,B), glycolytic flux (Figure 4A) and lactate secretion (Figure S5C). Accordingly, the expression of several genes involved in glycolysis and lactate metabolism, known to be regulated by HIF-1α, was altered in PHD2^{KD} cells (Figure S5D). In addition to stimulating glycolysis, PHD2^{KD} cells limited their OCR (Figure 2A), which was however not due to reduced glucose oxidation (Figure 4B), but can be explained by reduced fatty acid oxidation as evidenced by decreased palmitate β-oxidation in PHD2^{KD} cells (Figure 4C). Labeling with $^{13}C_6$-glucose revealed increased ^{13}C incorporation into glycolytic intermediates (phosphoenolpyruvate, pyruvate and lactate) and decreased incorporation into TCA cycle intermediates (citrate, α-KG, fumarate and malate) after PHD2 silencing (Figure S5H), confirming that enhanced HIF-1α-signaling limits glucose-derived carbons to enter the TCA cycle (DeBerardinis et al., 2008). This metabolic switch had no manifest effect on the energy state of PHD2^{KD} cells as ATP levels remained constant and p-AMPK levels on Western blot were not altered (Figures S5E,F). Together, these data indicate that PHD2-silenced periosteal cells switch to fermentative metabolism to support cellular bioenergetics (Figure S5G).

Glycogen Storage Is Vital for Bioenergetics and Survival of PHD2^{KD} mPDC During Glucose Deprivation

Glucose seems an important nutrient for PHD2^{KD} cells, as the consumption of this metabolite is increased (Figures S5A,B), whereas fatty oxidation is decreased (Figure 4C) and the increased glutamine uptake is shuttled to glutathione (Figure 3D) and not to the TCA cycle (Figure S4D). However, upon *in vivo* transplantation, the lack of blood vessels not only limits the availability of oxygen but also glucose, as passive diffusion is limited to 100-300 μm (Curcio et al., 2007; Phipps et al., 2015). We therefore questioned whether survival would be affected when PHD2^{KD} cells were deprived of this nutrient.

Despite the increased glucose consumption, PHD2^{KD} cells were manifestly more resistant to glucose deprivation (Figure 4D). A possible explanation is increased storage of glucose in the form of intracellular glycogen, allowing fast mobilization during nutrient deprivation. Indeed, PHD2^{KD} cells showed a 4-fold increase in glycogen deposition in the cytoplasm,

evidenced by periodic acid-Schiff (PAS) staining and biochemical titration of the glycogen content (Figures 4E,F). Moreover, PHD2^{KD} cells expressed significantly higher levels of genes involved in glycogen synthesis (phosphoglucomutase (*Pgm*) and glycogen synthase 1 (*Gys1*)) as well as breakdown (liver isoform of glycogen phosphorylase (*Pygl*)) (Figure S5I). During glucose deprivation, glycogen stores were fully exhausted in control cells, whereas PHD2^{KD} cells consumed 2 times more glycogen without depleting their stores (Figure 4G,H; compare white and grey bars). Gene expression analysis showed that especially PHD2^{KD} cells decreased *Gys* levels and increased *Pygl* levels during glucose deprivation, suggesting a shift in glycogen metabolism (Figure S5I). The importance of glycogen usage was investigated by treating cells with 1,4-dideoxy-1,4-imino-d-arabinitol (DAB), an inhibitor of PYGL, or silencing PYGL using shRNA (PHD2^{KD}PYGL^{KD}; Figure S5J), which prevented glycogen breakdown (Figures 4G,H). This strategy significantly abrogated the improved viability of PHD2^{KD} cells during glucose deprivation (Figures 4I,J). Mechanistically, inhibition of PYGL decreased ATP levels in glucose-deprived PHD2^{KD} cells (Figures S5K,L) and even resulted in an energy deficit as evidenced by decreased energy status (ATP/AMP levels; Figure 4K) and increased p-AMPK levels that reached the levels of glucose-deprived control cells (Figure 4L). On the other hand, PHD2^{KD} cells showed, compared to control cells, a smaller increase in ROS levels during glucose deprivation, which was however not affected by inhibition of PYGL (Figures 4M,N), but could be attributed to the increase in GLS1 (Figure S5M). Although the GLS1 activity is important for ROS scavenging during glucose deprivation, this pathway has no effect on ATP levels and only a marginal effect on cell survival in this condition (Figures S5N,O), indicating that preserving energy status by glycogen consumption is more important when cells are deprived from glucose. Indeed, silencing PYGL reduced the survival of implanted PHD2^{KD} cells also *in vivo* (Figure 4O), confirming that glycogen stores are crucial to maintain cell viability when nutrient supply is impaired.

The Combinational Changes in Glutamine and Glycogen Metabolism Are Necessary for PHD2^{KD} Cell Viability

Since PHD2^{KD} cells show improved survival during hypoxia (Figure 2H), we investigated how glutamine and glycogen metabolism contribute to this effect. Blocking GLS1 or PYGL decreased the viability of PHD2^{KD} cells in hypoxia, but not to the extent of control cells (Figures 5A,B), suggesting the involvement of both pathways. Indeed, glutamine metabolism was necessary for dampening ROS levels, while glycogen storage was important to maintain ATP levels, and no overlapping effects were observed (Figures 5C-F). Thus, inhibition of GLS1 or PYGL separately reduced the pro-survival capacity of PHD2^{KD} cells during respectively oxidative stress and glucose deprivation, whereas both pathways together regulate survival in hypoxia, by combining ROS scavenging and energy supply.

To mimic the *in vivo* stress conditions that cells experience upon implantation, we combined hypoxia, glucose deprivation and oxidative stress *in vitro*. Simultaneous knockdown of GLS1 and PYGL significantly reduced PHD2^{KD} cell survival during combined *in vitro* stress, and these results were confirmed by pharmacological intervention on PHD2-silenced cells using BPTES and DAB together (Figures S5P and 5G). These data were confirmed *in vivo* in the ectopic model as well as large bone defect, showing that silencing GLS1 and

PYGL together in implanted PHD2^{KD} cells reduced viability more strongly than single knockdowns as evidenced by AnxV-PI flow cytometry and TUNEL staining (Figures 5H,I and S5Q compared to 3I, 4O). Mechanistically, *in vivo* implanted PHD2^{KD}GLS1^{KD}PYGL^{KD} cells failed to increase the GSH:GSSG ratio, leading to high ROS levels (Figures 5J,K); and could not metabolize glycogen to avoid energy distress (Figures 5L,M).

Lastly, we questioned whether deletion of PHD2 in osteoprogenitors *in vivo* alters the metabolic phenotype of bone cells. To obtain skeletal progenitor cell-specific inactivation of PHD2, we crossed *Phd2$^{fl/fl}$* mice with *Osx1-GFP::Cre* mice. Deletion of PHD2 in skeletal progenitors (*Phd2^{osx-}*) phenocopied the key features observed in transplanted PHD2-silenced periosteal cells. Indeed, loss of *Phd2* resulted in accumulation of HIF-1α in the bone cells (Figures S6A,B) and was associated with increased trabecular bone mass (data not shown). Interestingly, we found that the expression of several important genes in glutamine (*Gls1*) and glycogen metabolism (*Pgm, Gys1, Pygl*) was increased in *Phd2^{osx-}* bones (Figure S6C), suggesting changes in bone cell metabolism. Indeed, the GSH:GSSG ratio was elevated, which was associated with low intracellular ROS levels (Figures S6D,E). Moreover, intracellular glycogen content was increased (Figure S6F).

Thus, the combination of glutamine and glycogen metabolism is crucial for PHD2^{KD} cell survival under hypoxic and nutritional stress.

HIF-1α Mediates the Positive Effects on Cell Survival and Bone Regeneration in PHD2^{KD} mPDC

The data discussed indicate that PHD2 silencing results in increased HIF-1α levels. To ascertain that HIF-1α activation was causing these effects, we genetically silenced HIF-1α in PHD2^{KD} cells (PHD2^{KD}HIF-1α^{KD}) using shRNA, a strategy that did not affect HIF-2α levels (Figures 6A and S7A). Knockdown of HIF-1α significantly reduced the viability of PHD2^{KD} cells to the level of control cells both in the two *in vivo* models and during *in vitro* stress conditions (Figures 6B-E and S7B-D). Mechanistically, PHD2^{KD}HIF-1α^{KD} cells failed to increase *in vivo* and *in vitro* the GSH:GSSG ratio (Figures 6F,G), leading to increased ROS levels (Figures 6H,I). Moreover, these cells did not increase glycogen storage *in vivo* nor *in vitro* (Figures 6J-L), causing energy distress (Figure 6M). The increase in mRNA levels of metabolic enzymes and transporters observed in PHD2^{KD} cells was abrogated in PHD2^{KD}HIF-1α^{KD} cells (Table S1). In contrast, silencing of HIF-2α (Figure S7E) had no effect on the expression of these genes (Table 1S), nor did it alter ROS levels during normal culture conditions or during *in vitro* stress (Figures S7F,G). To investigate whether key genes in glutamine (*Gls1*) and glycogen (*Gys1*, *Pygl*) metabolism were directly transcriptionally regulated by HIF-1α in PHD2^{KD} cells, we performed HIF-1β ChIP-quantitative PCR (ChIP-qPCR) after silencing HIF-2α. We observed a significant enrichment of HIF-1 β binding to the promotor region of known HIF-1α target genes, including *Ldh-a, Pdk1* and *Gys1* (Figure 6N). In addition, we identified *Pygl* as a novel HIF-1 α target, whereas *Gls1* appeared not directly regulated by HIF-1α at the interrogated target site (Figure 6N). Lastly, we questioned whether *in vitro* stress conditions increased HIF-1α-dependent signaling. Only hypoxic culture, but not H_2O_2-treatment or glucose

deprivation, stabilized HIF-1α and induced HIF-regulated gene expression in control cells, but had no additional effect on gene expression in $PHD2^{KD}$ cells (Figures S7H-M).

The central role of HIF-1α in PHD2-silenced cells was further evidenced by the reduced *in vivo* bone formation 8 weeks after implantation, associated with a decreased angiogenic response (Figures 6O and S7N). Thus, the enhanced survival and bone forming potential of PHD2-silenced cells is HIF-1α dependent.

Pharmacological Inactivation of PHDs Mirrors the Effects Observed in $PHD2^{KD}$ mPDC

Finally, we investigated whether pharmacological blockade of PHDs recapitulates the effects of genetically silencing PHD2, by treating periosteal cells with JNJ-42041935 (JNJ) or IOX2. JNJ and IOX2 increased HIF-1α levels in wild-type mPDC (Figure 7A), thereby stimulating the expression of genes regulated by HIF-1α (Table S2). Treatment with these compounds increased the GSH:GSSG ratio (Figure 7B), resulting in decreased basal and H_2O_2-induced ROS levels (Figures 7C). They also enhanced *Pgm* and *Gys1* gene expression (Table S2), causing increased glycogen storage (Figure 7D). Finally, we observed that pharmacological blockade of PHD2 significantly increased the number of viable cells during combined *in vitro* stress (Figure 7E). This improved cell survival was mediated by GLS1 and PYGL, as treatment with BPTES and DAB abrogated the pro-survival effect (Figure 7F). Pharmacological inhibition of PHDs in periosteal cells prior to implantation also markedly improved survival in the two *in vivo* models (Figures 7G,H), which could be even further enhanced by additional local administration of the inhibitors (Figure 7G). Confirming the genetic approach, IOX2-treated cells exhibited an increase in the GSH:GSSG ratio, necessary to dampen ROS levels (Figures 7I,J); and accumulated intracellular glycogen to serve as an energy storage (Figures 7K,L).

Taken together, we discovered that adaptations in glutamine and glycogen metabolism can improve the clinical outcome of cell-based therapies for bone regeneration.

Discussion

The poor survival of cells implanted in ischemic and hypoxic tissues seriously compromises the success rate of cell-based regenerative medicine. The present study provides strong evidence that combined adaptations in glutamine and glucose metabolism in response to HIF-1α signaling are required to increase the viability of implanted periosteal cells. Indeed, PHD2 silencing enhances ROS scavenging through GLS1-dependent conversion of glutamine into glutathione and increases glycogen stores that serve as energy depots, thereby providing cells with metabolic advantages to survive and improve tissue repair.

Despite increasing research in bone tissue engineering, the healing of large bone defects remains a medical challenge as most of the implanted cells will undergo cell death. Until now, the beneficial effects of hypoxic preconditioning of cells have been studied in non-skeletal tissue regeneration and have mainly been attributed to the attraction of blood vessels and host cells, which are rather late effects. In the present study, we show that activation of the HIF signaling pathway in skeletal progenitors prior to implantation improved their survival, not by accelerating vascular ingrowth in these early phases but by adapting cellular

metabolism of glutamine and glucose to endure the limited supply of oxygen and nutrients. Interestingly, glucose and glutamine were each used for a specific metabolic goal; glucose for bioenergetics and glutamine for redox balance. Glutamine uptake was increased in PHD2-silenced skeletal cells and was converted into glutathione. Higher levels of this potent antioxidant were required to detoxify the increased ROS levels during hypoxia and glucose deprivation. Indeed, blockade of GLS1 in $PHD2^{KD}$ cells markedly attenuated glutathione levels and increased ROS levels and cell death, but addition of glutamate rescued the survival of these cells during *in vitro* stress conditions.

The conversion of glutamine specifically to glutathione differs from the use of glutamine in hypoxic cancer cells. In tumor cells, glutamine regulates cell survival and proliferation mainly via anaplerotic entry in the TCA cycle and reductive carboxylation, contributing to the biosynthetic and bioenergetic demands of these cells (Le et al., 2012; Gameiro et al., 2013; Wise et al., 2011; Metallo et al., 2012). In contrast, activation of the HIF pathway in skeletal progenitor cells decreased glutamine anaplerosis in the TCA cycle, and did not induce reductive carboxylation (data not shown). Accordingly, pharmacological or genetic blockade of GLS1, in $PHD2^{KD}$ cells had no effect on ATP levels. Moreover, the addition of TCA cycle intermediates was not able to rescue $PHD2^{KD}$ cell death during *in vitro* stress conditions when GLS1 was inhibited. These results are in line with recent observations in glutamate dehydrogenase 1-silenced cells, where the decrease in glutamine anaplerosis did not alter ATP production (Jin et al., 2015). Thus, glutamine-dependent reductive carboxylation or TCA cycle anaplerosis seems less critical for cells that show low proliferation rates and/or that depend on other pathways, like glucose metabolism, to sustain bioenergetics.

In addition to preserving redox balance, cells require specific metabolic alterations to meet their bioenergetic needs for surviving nutrient depletion. Activating HIF signaling in skeletal progenitor cells resulted in a more than 4-fold increase in glycogen content. Consumption of the stored glycogen during prolonged stress conditions prevented an energetic crisis and cell death. These data are consistent with previous observations in cancer and non-malignant cells where hypoxia-induced glycogen serves as an energy store (Pelletier et al., 2012; Pescador et al., 2010; Zhu et al., 2014). Importantly, in skeletal cells, the inhibition of glycogen consumption by genetic or pharmacological inhibition of PYGL had no effect on ROS levels, further emphasizing the importance of glutamine to maintain redox balance. These data differ from findings in cancer cells, where glycogen consumption also provides NADPH through the pentose-phosphate pathway and thereby prevents ROS-induced cell cycle arrest (Favaro et al., 2012). The present findings also reveal that skeletal progenitors contain already a substantial amount of glycogen, which may fit with the observation that glycolysis is important for osteoblast differentiation (Esen et al., 2013; Regan et al., 2014). The presence of glycogen may be a safeguard to protect these high glucose consuming cells during deprivation and the hypoxia-induced increase in glycogen storage likely helps to anticipate a future threat of energy starvation.

Our results suggest that the molecular, cellular and *in vivo* biological effects induced by PHD2 inactivation in periosteal cells are largely dependent on HIF-1α signaling, as concurrent HIF-1 α silencing reverted the increase in *Gys1, Pygl* and *Gls1* gene

transcription, blocked the adaptations in glutamine and glycogen metabolism, and abolished the pro-survival effect of PHD2^{KD} in implanted periosteal cells. In addition, our ChIP-PCR data strongly suggest that the transcription of *Gys1* and *Pygl* was directly regulated by HIF-1α, whereas *Gls1* appeared not to be a direct HIF-1α target in PHD2^{KD} periosteal cells. Understanding the molecular mechanisms by which HIF regulates gene transcription in normal and diseased conditions is an important topic of ongoing research. Indeed, recent evidence shows that cell type-specific patterns of chromatin structure influence the range of HIF target genes (Schodel et al., 2011) and that other stress-responsive transcription factors that bind in the proximity of a HIF-1α binding site can modulate its interaction with the hypoxia responsive element of the target gene or with the transcriptional machinery (Keith et al., 2012; Villar et al., 2012). Although we show that the expression of *Gys1, Pygl* and *Gls1* in PHD2^{KD} periosteal cells exposed to hypoxia, glucose deprivation or oxidative stress remains mainly HIF-1α dependent, future investigations are necessary to characterize the mechanisms that fine-tune the HIF transcriptional response during stress conditions.

Collectively, we propose that HIF-1α-dependent concurrent changes in glutamine and glycogen metabolism are crucial for cell survival and contribute to increased bone formation. Pharmacological inhibition of PHD2 provides proof-of-principle that the strategy of improved cell survival through metabolic reprogramming may stimulate regeneration, indicating that this approach may also be applicable to other models of delayed repair, including skin, heart and skeletal muscle (Maxson et al., 2012).

Experimental Procedures

More detailed methods are described in the Supplemental Experimental Procedures.

Animals and Cell Culture

Phd2$^{fl/fl}$ mice were generated as described before (Mazzone et al., 2009) and were bred in conventional conditions in our animal housing facility (Proefdierencentrum Leuven, Belgium). Housing and experimental procedures were approved by the Institutional Animal Care and Research Advisory Committee of the KU Leuven. Murine periosteal progenitor cells were isolated according to the protocol described previously (van Gastel et al., 2012) and cultured in αMEM with 2 mM glutaMAX™-1, containing 1% penicillin/streptomycin and 10% fetal bovine serum (FBS).

Mouse Models

To analyze *in vivo* cell survival and bone formation, periosteal cell were seeded onto a calcium phosphate-collagen scaffold and implanted subcutaneously or in a non-healing tibial defect in nude mice (van Gastel et al., 2014). After three days, we assessed cell survival via histological and AnxV-PI flow cytometry analyses. Bone formation was assessed 8 weeks after implantation by histological analysis.

(Immuno)Histochemistry and Histomorphometry

Histochemical (H&E) and immunohistochemical CD31, TUNEL and Hypoxyprobe-1 stainings were described previously (Maes et al., 2012; van Gastel et al., 2012; van Gastel et

al., 2014). Assessment and morphometric quantification of apoptosis, hypoxia and oxidative DNA damage were performed as described in the Supplemental Experimental Procedures.

RNA and Protein Expression Analysis

RNA isolation and subsequent qRT-PCR analysis as well as protein extraction and Western blot analysis were performed as described before (van Gastel et al., 2012; van Gastel et al., 2014).

Metabolism Assays

Oxygen consumption was measured using the Seahorse XF24 analyzer. GSH, GSSG and total glutathione levels were measured using the Glutathione Fluorometric Assay Kit following manufacturer's instructions. ROS levels were determined using MitoSOX Red (mitochondrial superoxides) or CM-H_2DCFDA (total intracellular ROS). Glycolysis, glucose oxidation and fatty acid oxidation were measured after incubating cells with the appropriate radioactive-labeled tracer ([5-^{3}H]-D-glucose, [6-^{14}C]-D-glucose or [9,10-^{3}H]-palmitate, respectively). ^3H_2O derived from glucose or palmitate was a measure for glycolytic flux or fatty acid oxidation, respectively; $^{14}CO_2$ derived from glucose was a measure for glucose oxidation. Energy status was calculated as the ratio of ATP over AMP after high-performance liquid chromatography measurement in cell extracts. Intracellular ATP levels were also measured using the ATPlite ATP detection assay. Glycogen levels were determined using a Glycogen Assay Kit or visualized by PAS staining.

Analysis of ^{13}C-labeled Metabolites

For metabolite analysis using mass spectrometry, cells were cultured for 24 hours in glucose- and glutamine-free αMEM with dialyzed FBS and the appropriate tracer added. [U-$^{13}C_5$]glutamine and [U-$^{13}C_6$]glucose were from Sigma-Aldrich and Cambridge Isotopes Laboratories, Inc., respectively. Samples were extracted and analyzed as described in the Supplemental Experimental Procedures.

Statistics

Data are presented as means ± SEM. Data were analyzed by two-sided two-sample Student's *t*-test, and one-way or two-way ANOVA with Tukey-Kramer post-hoc test using the NCSS statistical software. Differences were considered statistically significant at $p<0.05$.

Supplementary Material

Refer to Web version on PubMed Central for supplementary material.

Acknowledgements

The authors wish to thank I. Stockmans, K. Moermans and B. Vanwetswinkel for technical assistance, M. Depypere for MeVisLab software, D. Verdegem for isotopomer distribution software, C. Mathieu for Gallios™ flow cytometer use and M. Mazzone for hypoxia incubator use. G.C. acknowledges funding from Fund for Scientific Research-Flanders (FWO: G.0835.11, G.0A72.13 and G.096414); P.C. from longterm structural funding – Methusalem Funding by the Flemish Government; S.-M.F. from Marie Curie-CIG, FWO-Odysseus, Concern Foundation, FWO-Research Grants, E. Yourassowsky Schenking, and Bayer Health Care. S.S. is fellow from the Agency for Innovation by Science and Technology in Flanders (IWT). N.v.G. is funded by KUL-GOA 3M120209.

This work is part of Prometheus, the KU Leuven R&D Division of Skeletal Tissue Engineering. The authors declare no conflict of interest.

References

Aragones J, Fraisl P, Baes M, Carmeliet P. Oxygen sensors at the crossroad of metabolism. Cell Metab. 2009; 9:11–22. [PubMed: 19117543]

Buescher JM, Antoniewicz MR, Boros LG, Burgess SC, Brunengraber H, Clish CB, DeBerardinis RJ, Feron O, Frezza C, Ghesquiere B, Gottlieb E, et al. A roadmap for interpreting C metabolite labeling patterns from cells. Curr Opin Biotechnol. 2015; 34C:189–201.

Curcio E, Salerno S, Barbieri G, De Bartolo L, Drioli E, Bader A. Mass transfer and metabolic reactions in hepatocyte spheroids cultured in rotating wall gas-permeable membrane system. Biomaterials. 2007; 28:5487–5497. [PubMed: 17881050]

DeBerardinis RJ, Lum JJ, Hatzivassiliou G, Thompson CB. The biology of cancer: metabolic reprogramming fuels cell growth and proliferation. Cell Metab. 2008; 7:11–20. [PubMed: 18177721]

Esen E, Chen J, Karner CM, Okunade AL, Patterson BW, Long F. WNT-LRP5 signaling induces Warburg effect through mTORC2 activation during osteoblast differentiation. Cell Metab. 2013; 17:745–755. [PubMed: 23623748]

Favaro E, Bensaad K, Chong MG, Tennant DA, Ferguson DJ, Snell C, Steers G, Turley H, Li JL, Gunther UL, Buffa FM, et al. Glucose utilization via glycogen phosphorylase sustains proliferation and prevents premature senescence in cancer cells. Cell Metab. 2012; 16:751–764. [PubMed: 23177934]

Francis KR, Wei L. Human embryonic stem cell neural differentiation and enhanced cell survival promoted by hypoxic preconditioning. Cell Death Dis. 2010; 1 e22 [PubMed: 21364630]

Gameiro PA, Yang J, Metelo AM, Perez-Carro R, Baker R, Wang Z, Arreola A, Rathmell WK, Olumi A, Lopez-Larrubia P, Stephanopoulos G, et al. In vivo HIF-mediated reductive carboxylation is regulated by citrate levels and sensitizes VHL-deficient cells to glutamine deprivation. Cell Metab. 2013; 17:372–385. [PubMed: 23473032]

Grayson WL, Bunnell BA, Martin E, Frazier T, Hung BP, Gimble JM. Stromal cells and stem cells in clinical bone regeneration. Nat Rev Endocrinol. 2015; 11:140–150. [PubMed: 25560703]

Guzy RD, Hoyos B, Robin E, Chen H, Liu L, Mansfield KD, Simon MC, Hammerling U, Schumacker PT. Mitochondrial complex III is required for hypoxia-induced ROS production and cellular oxygen sensing. Cell Metab. 2005; 1:401–408. [PubMed: 16054089]

Hanahan D, Weinberg RA. Hallmarks of cancer: the next generation. Cell. 2011; 144:646–674. [PubMed: 21376230]

Hansson EM, Lindsay ME, Chien KR. Regeneration next: toward heart stem cell therapeutics. Cell Stem Cell. 2009; 5:364–377. [PubMed: 19796617]

Jain RK, Au P, Tam J, Duda DG, Fukumura D. Engineering vascularized tissue. Nat Biotechnol. 2005; 23:821–823. [PubMed: 16003365]

Jin L, Li D, Alesi GN, Fan J, Kang HB, Lu Z, Boggon TJ, Jin P, Yi H, Wright ER, Duong D, et al. Glutamate Dehydrogenase 1 Signals through Antioxidant Glutathione Peroxidase 1 to Regulate Redox Homeostasis and Tumor Growth. Cancer Cell. 2015; 27:257–270. [PubMed: 25670081]

Keith B, Johnson RS, Simon MC. HIF1alpha and HIF2alpha: sibling rivalry in hypoxic tumour growth and progression. Nat Rev Cancer. 2012; 12:9–22.

Kim HW, Haider HK, Jiang S, Ashraf M. Ischemic preconditioning augments survival of stem cells via miR-210 expression by targeting caspase-8-associated protein 2. J Biol Chem. 2009; 284:33161–33168. [PubMed: 19721136]

Laschke MW, Harder Y, Amon M, Martin I, Farhadi J, Ring A, Torio-Padron N, Schramm R, Rucker M, Junker D, Haufel JM, et al. Angiogenesis in tissue engineering: breathing life into constructed tissue substitutes. Tissue Eng. 2006; 12:2093–2104. [PubMed: 16968151]

Le A, Lane AN, Hamaker M, Bose S, Gouw A, Barbi J, Tsukamoto T, Rojas CJ, Slusher BS, Zhang H, Zimmerman LJ, et al. Glucose-independent glutamine metabolism via TCA cycling for proliferation and survival in B cells. Cell Metab. 2012; 15:110–121. [PubMed: 22225880]

Liu H, Liu S, Li Y, Wang X, Xue W, Ge G, Luo X. The role of SDF-1-CXCR4/CXCR7 axis in the therapeutic effects of hypoxia-preconditioned mesenchymal stem cells for renal ischemia/reperfusion injury. PLoS One. 2012; 7 e34608 [PubMed: 22511954]

Maes C, Araldi E, Haigh K, Khatri R, Van Looveren R, Giaccia AJ, Haigh JJ, Carmeliet G, Schipani E. VEGF-independent cell-autonomous functions of HIF-1alpha regulating oxygen consumption in fetal cartilage are critical for chondrocyte survival. J Bone Miner Res. 2012; 27:596–609. [PubMed: 22162090]

Maxson S, Lopez EA, Yoo D, Danilkovitch-Miagkova A, Leroux MA. Concise review: role of mesenchymal stem cells in wound repair. Stem Cells Transl Med. 2012; 1:142–149. [PubMed: 23197761]

Mazzone M, Dettori D, Leite de Oliveira R, Loges S, Schmidt T, Jonckx B, Tian YM, Lanahan AA, Pollard P, Ruiz de Almodovar C, De Smet F, et al. Heterozygous deficiency of PHD2 restores tumor oxygenation and inhibits metastasis via endothelial normalization. Cell. 2009; 136:839–851. [PubMed: 19217150]

Metallo CM, Gameiro PA, Bell EL, Mattaini KR, Yang J, Hiller K, Jewell CM, Johnson ZR, Irvine DJ, Guarente L, Kelleher JK, et al. Reductive glutamine metabolism by IDH1 mediates lipogenesis under hypoxia. Nature. 2012; 481:380–384.

Muscari C, Giordano E, Bonafe F, Govoni M, Pasini A, Guarnieri C. Priming adult stem cells by hypoxic pretreatments for applications in regenerative medicine. J Biomed Sci. 2013; 20:63. [PubMed: 23985033]

Muschler GF, Nakamoto C, Griffith LG. Engineering principles of clinical cellbased tissue engineering. J Bone Joint Surg Am. 2004; 86-A:1541–1558.

Pelletier J, Bellot G, Gounon P, Lacas-Gervais S, Pouyssegur J, Mazure NM. Glycogen Synthesis is Induced in Hypoxia by the Hypoxia-Inducible Factor and Promotes Cancer Cell Survival. Front Oncol. 2012; 2:18. [PubMed: 22649778]

Pescador N, Villar D, Cifuentes D, Garcia-Rocha M, Ortiz-Barahona A, Vazquez S, Ordonez A, Cuevas Y, Saez-Morales D, Garcia-Bermejo ML, Landazuri MO, et al. Hypoxia promotes glycogen accumulation through hypoxia inducible factor (HIF)-mediated induction of glycogen synthase 1. PLoS One. 2010; 5 e9644 [PubMed: 20300197]

Phipps C, Molavian H, Kohandel M. A microscale mathematical model for metabolic symbiosis: Investigating the effects of metabolic inhibition on ATP turnover in tumors. J Theor Biol. 2015; 366:103–114. [PubMed: 25433213]

Regan JN, Lim J, Shi Y, Joeng KS, Arbeit JM, Shohet RV, Long F. Upregulation of glycolytic metabolism is required for HIF1alpha-driven bone formation. Proc Natl Acad Sci U S A. 2014; 111:8673–8678. [PubMed: 24912186]

Rosado-de-Castro PH, Schmidt FR, Battistella V, Lopes de Souza SA, Gutfilen B, Goldenberg RC, Kasai-Brunswick TH, Vairo L, Silva RM, Wajnberg E, Alvarenga Americano do Brasil PE, et al. Biodistribution of bone marrow mononuclear cells after intra-arterial or intravenous transplantation in subacute stroke patients. Regen Med. 2013; 8:145–155. [PubMed: 23477395]

Rouwkema J, Rivron NC, van Blitterswijk CA. Vascularization in tissue engineering. Trends Biotechnol. 2008; 26:434–441. [PubMed: 18585808]

Schodel J, Oikonomopoulos S, Ragoussis J, Pugh CW, Ratcliffe PJ, Mole DR. High-resolution genome-wide mapping of HIF-binding sites by ChIP-seq. Blood. 2011; 117:e207–e217. [PubMed: 21447827]

Semenza GL. HIF-1 mediates metabolic responses to intratumoral hypoxia and oncogenic mutations. J Clin Invest. 2013; 123:3664–3671. [PubMed: 23999440]

Shen X, Wan C, Ramaswamy G, Mavalli M, Wang Y, Duvall CL, Deng LF, Guldberg RE, Eberhart A, Clemens TL, Gilbert SR. Prolyl hydroxylase inhibitors increase neoangiogenesis and callus formation following femur fracture in mice. J Orthop Res. 2009; 27:1298–1305. [PubMed: 19338032]

Stegen S, van Gastel N, Carmeliet G. Bringing new life to damaged bone: the importance of angiogenesis in bone repair and regeneration. Bone. 2015; 70:19–27. [PubMed: 25263520]

van Gastel N, Stegen S, Stockmans I, Moermans K, Schrooten J, Graf D, Luyten FP, Carmeliet G. Expansion of murine periosteal progenitor cells with fibroblast growth factor 2 reveals an intrinsic

endochondral ossification program mediated by bone morphogenetic protein 2. Stem Cells. 2014; 32:2407–2418. [PubMed: 24989687]

van Gastel N, Torrekens S, Roberts SJ, Moermans K, Schrooten J, Carmeliet P, Luttun A, Luyten FP, Carmeliet G. Engineering vascularized bone: osteogenic and proangiogenic potential of murine periosteal cells. Stem Cells. 2012; 30:2460–2471. [PubMed: 22911908]

Villar D, Ortiz-Barahona A, Gomez-Maldonado L, Pescador N, Sanchez-Cabo F, Hackl H, Rodriguez BA, Trajanoski Z, Dopazo A, Huang TH, Yan PS, et al. Cooperativity of stress-responsive transcription factors in core hypoxia-inducible factor binding regions. PLoS One. 2012; 7 e45708 [PubMed: 23029193]

Wan C, Gilbert SR, Wang Y, Cao X, Shen X, Ramaswamy G, Jacobsen KA, Alaql ZS, Eberhardt AW, Gerstenfeld LC, Einhorn TA, et al. Activation of the hypoxia-inducible factor-1alpha pathway accelerates bone regeneration. Proc Natl Acad Sci U S A. 2008; 105:686–691. [PubMed: 18184809]

Waypa GB, Marks JD, Guzy R, Mungai PT, Schriewer J, Dokic D, Schumacker PT. Hypoxia triggers subcellular compartmental redox signaling in vascular smooth muscle cells. Circ Res. 2010; 106:526–535. [PubMed: 20019331]

Wise DR, Ward PS, Shay JE, Cross JR, Gruber JJ, Sachdeva UM, Platt JM, DeMatteo RG, Simon MC, Thompson CB. Hypoxia promotes isocitrate dehydrogenase-dependent carboxylation of alpha-ketoglutarate to citrate to support cell growth and viability. Proc Natl Acad Sci U S A. 2011; 108:19611–19616. [PubMed: 22106302]

Zheng X, Zheng X, Wang X, Ma Z, Gupta SV, Botusan I, Takeda T, Bjorklund A, Inoue M, Catrina SB, Brismar K, et al. Acute hypoxia induces apoptosis of pancreatic beta-cell by activation of the unfolded protein response and upregulation of CHOP. Cell Death Dis. 2012; 3 e322 [PubMed: 22695615]

Zhu H, Sun A, Zou Y, Ge J. Inducible metabolic adaptation promotes mesenchymal stem cell therapy for ischemia: a hypoxia-induced and glycogen-based energy prestorage strategy. Arterioscler Thromb Vasc Biol. 2014; 34:870–876. [PubMed: 24558105]

Europe PMC Funders Author Manuscripts

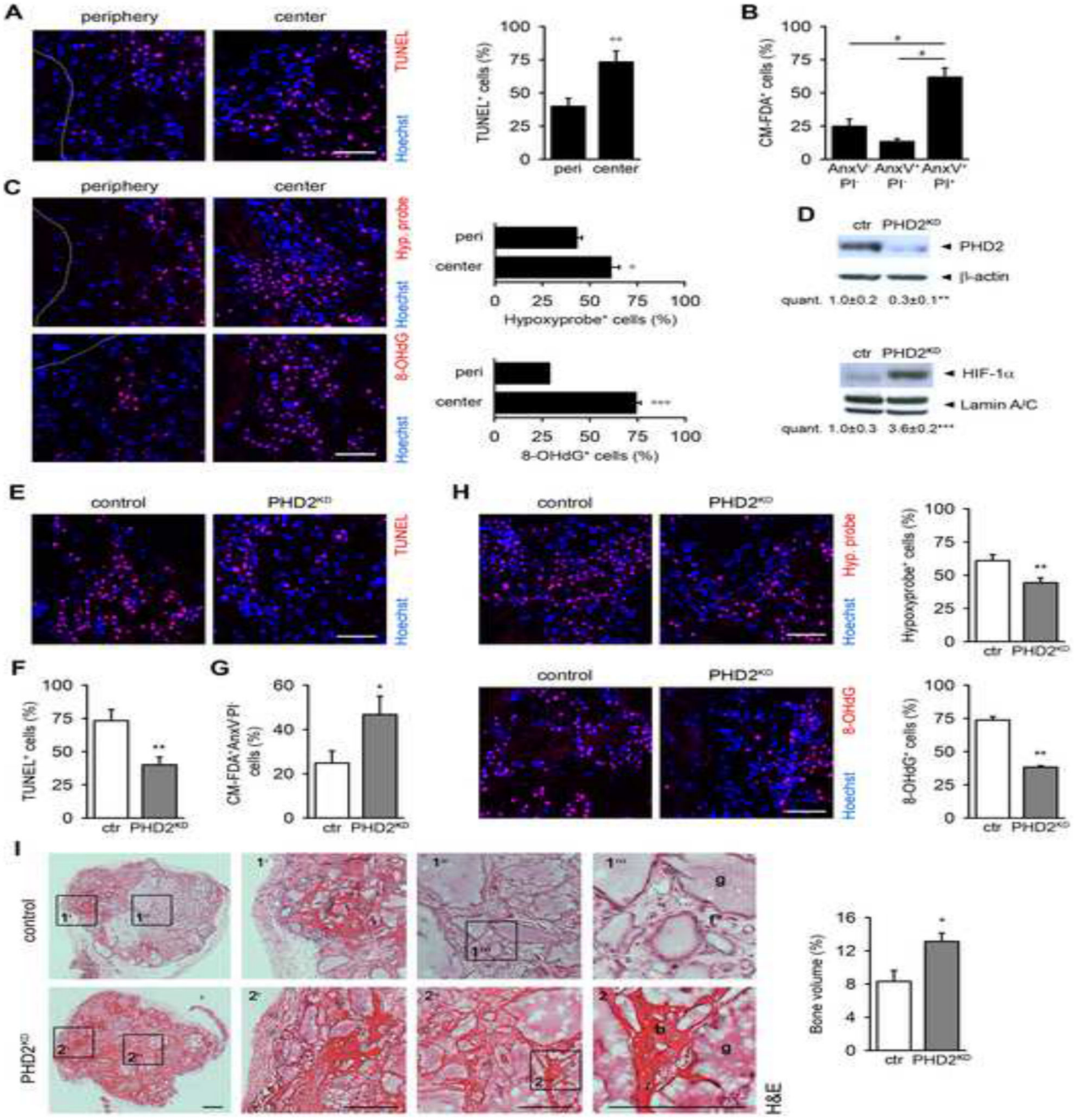

Figure 1. Deletion of PHD2 Improves Cell Survival and Bone Regeneration

(A) TUNEL immunostaining of scaffolds seeded with mouse periosteum-derived cells (mPDC), and quantification at the periphery (peri) or center (n=4).

(B) *Ex vivo* Annexin V-PI (AnxV-PI) flow cytometry analysis of CM-FDA-labeled implanted cells (n=3).

(C) Hypoxyprobe (Hyp. probe) and 8-OHdG immunostaining, and quantification at the periphery or center (n=4).

Europe PMC Funders Author Manuscripts

(D) PHD2, β-actin, HIF-1α and Lamin A/C immunoblot on mPDC lysates, 3 days after transduction of *Phd2*$^{fl/fl}$ cells with Ad-GFP (control; ctr) or Ad-Cre (PHD2^{KD}) (n=3).
(E-F) TUNEL immunostaining (E) with quantification (F) in the scaffold center (n=8).
(G) *Ex vivo* quantification of the viable implanted (CM-FDA^{+}AnxV^{-}PI^{-} cells (n=3-4).
(H) Hypoxyprobe and 8-OHdG immunostaining of the center of the scaffold (n=4), with quantification.
(I) H&E staining with quantification of the newly formed bone in the total scaffold (n=8). Boxed areas at the periphery (1', 2') or center (1", 2") are subsequently magnified (b, bone; f, fibrous tissue; g, scaffold granule).
A-C and E-H: analysis at day 3 after implantation; I, after 8 weeks. Scale bars: 100 μm in A, C, E and H; 500 μm in I. Dotted lines indicate scaffold boundaries. Data are means ± SEM. °p<0.05 vs. peri, °°p<0.01 vs. peri, °°°p<0.001 vs. peri, *p<0.05 vs. ctr, **p<0.01 vs. ctr, ***p<0.001 vs. ctr (Student's *t*-test), #p<0.05 (ANOVA).

Europe PMC Funders Author Manuscripts

Europe PMC Funders Author Manuscripts

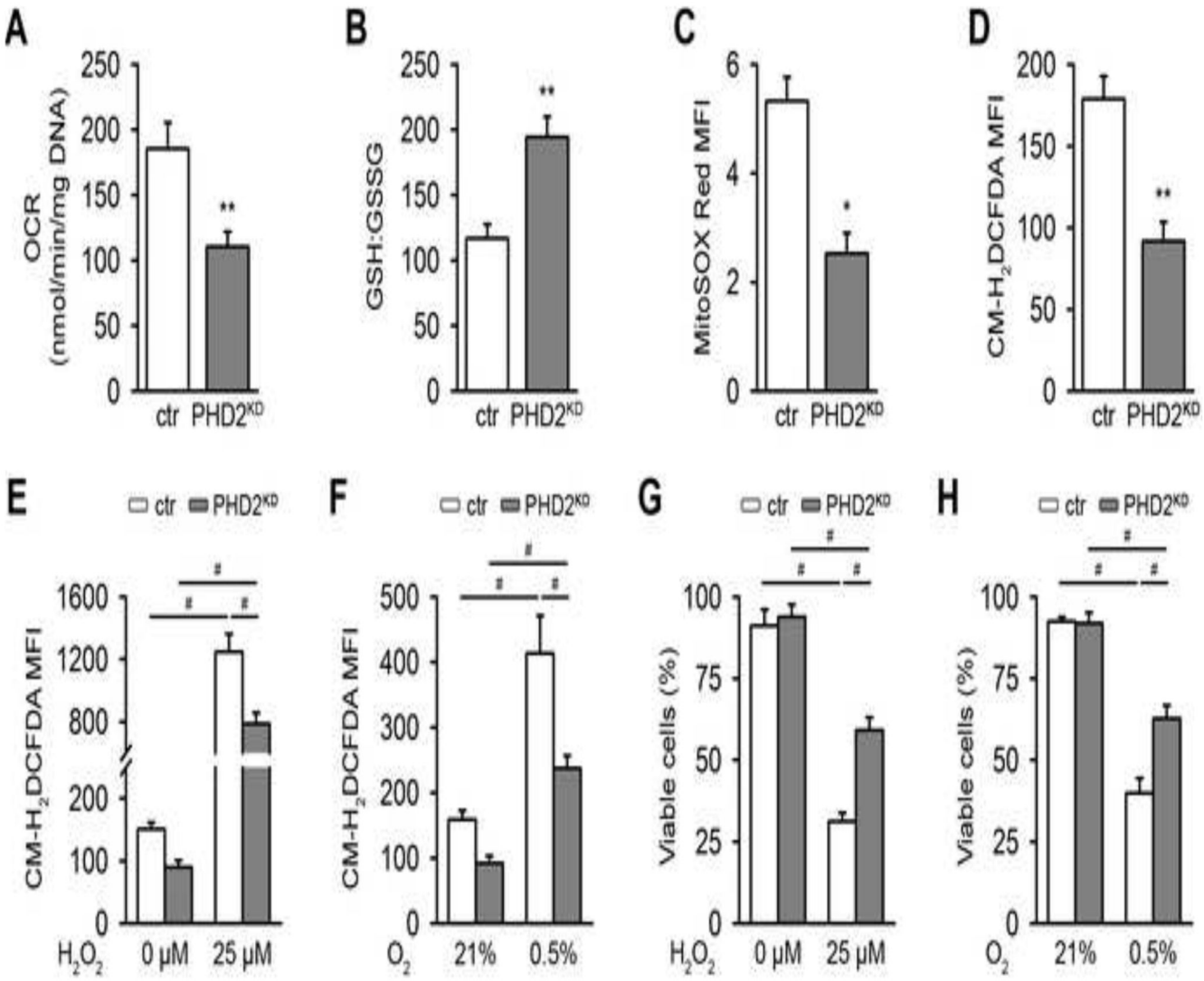

Figure 2. PHD2^{KD} Cells Are Metabolically Reprogrammed

(A) Basal oxygen consumption rate (OCR) of cultured control (ctr) and PHD2^{KD} mPDC (n=6).

(B) Ratio of reduced glutathione (GSH) to oxidized glutathione (GSSG) (n=6).

(C-D) Mean fluorescent intensity (MFI) of mitochondrial (MitoSOX Red; C) or intracellular ROS levels (CM-H_2DCFDA; D) by flow cytometry analysis (n=6-9).

(E-F) Intracellular ROS levels after treatment with 25 µM H_2O_2 (E) or culture in 0.5% oxygen (O_2; F) (n=6).

(G-H) Cell viability analysis after treatment with 25 µM H_2O_2 (G) or culture in 0.5% O_2 (H), by AnxV-PI flow cytometry (n=9).

Data are means ± SEM. *p<0.05 vs. ctr, **p<0.01 vs. ctr (Student's t-test), #p<0.05 (ANOVA).

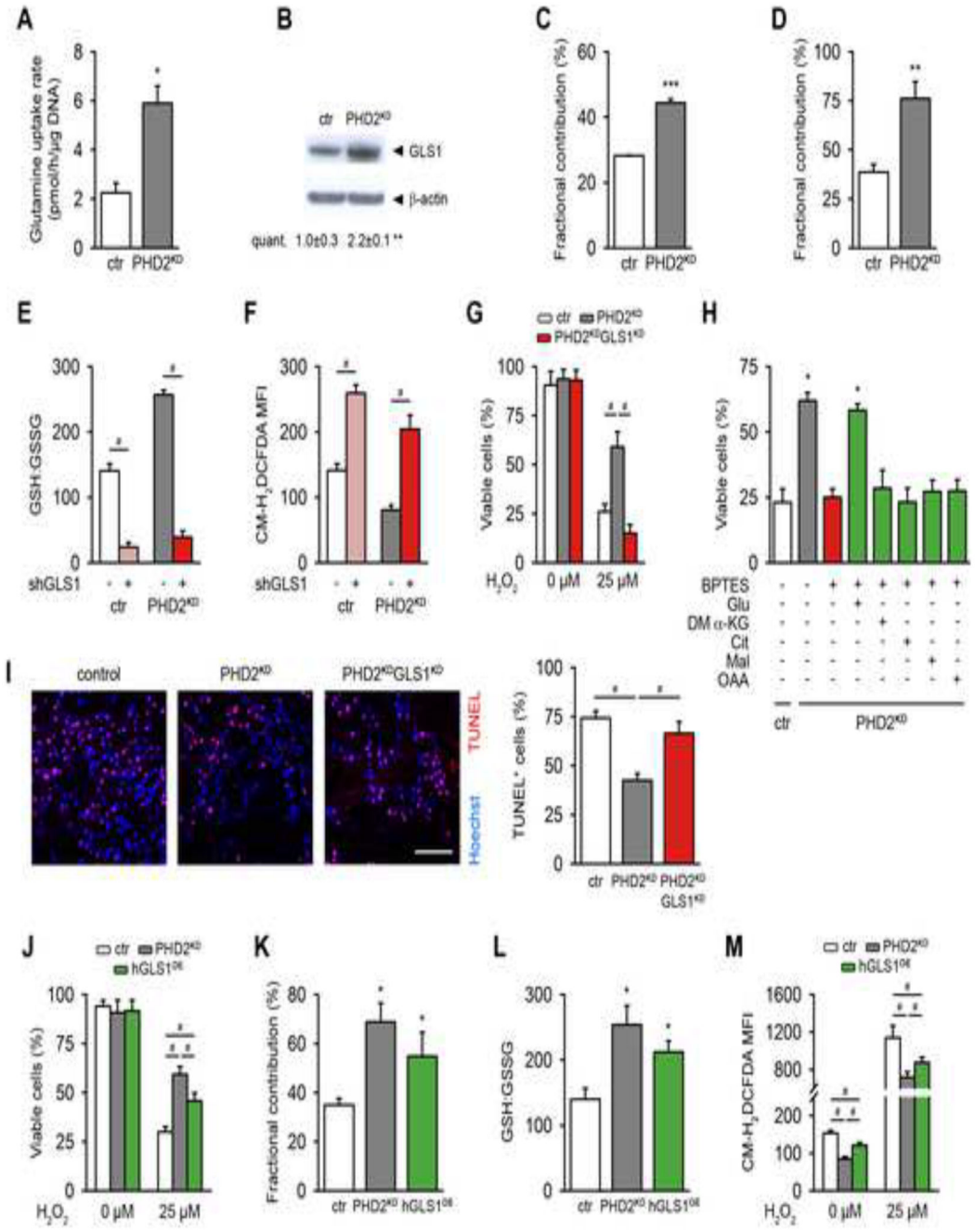

Figure 3. GLS1 Regulates Glutamine-mediated ROS Scavenging in PHD2^{KD} Cells and Contributes to Cell Survival

(A) Glutamine uptake rate in cultured control (ctr) and PHD2^{KD} cells (n=6).

(B) GLS1 and β-actin immunoblot (n=3).

(C-D) Fractional contribution of [U-^{13}C]-glutamine to glutamate (C) and GSH (D) (n=3-6).

(E-F) GSH to GSSG levels (E) and total intracellular ROS levels (F) in control and PHD2^{KD} cells after genetic silencing of GLS1 (scrambled shRNA (shScr: -) or shGLS1 (+)) (n=6).

(G) Control, PHD2^{KD} and PHD2^{KD}GLS1^{KD} cell viability after treatment with 25 μM H_2O_2 (n=6). PHD2^{KD}GLS1^{KD} cells are PHD2^{KD} cells transduced with shGLS1; ctr and PHD2^{KD} cells are transduced with shScr.

(H) Rescue of cell viability of BPTES-treated PHD2^{KD} cells during oxidative stress (25 μM H_2O_2) with glutamate (Glu), but not with dimethyl α-ketoglutarate (DM α-KG), citrate (Cit), malate (Mal) or oxaloacetate (OAA) (n=9).

(I) TUNEL immunostaining of the scaffold center 3 days after implantation, and quantification (scale bar, 100 μm; n=4).

(J) Cell viability of control, PHD2^{KD} and hGLS1-overexpressing (hGLS1^{OE}) cells after treatment with 25 μM H_2O_2 (n=6).

(K) Fractional contribution of [U-^{13}C]-glutamine to GSH (n=6).

(L) Ratio of GSH to GSSG (n=6).

(M) Total intracellular ROS levels with and without H_2O_2 treatment (n=6).

Data are means ± SEM. *p<0.05 vs. ctr, **p<0.01 vs. ctr, ***p<0.001 vs. ctr (Student's *t*-test), #p<0.05 (ANOVA).

Europe PMC Funders Author Manuscripts

Europe PMC Funders Author Manuscripts

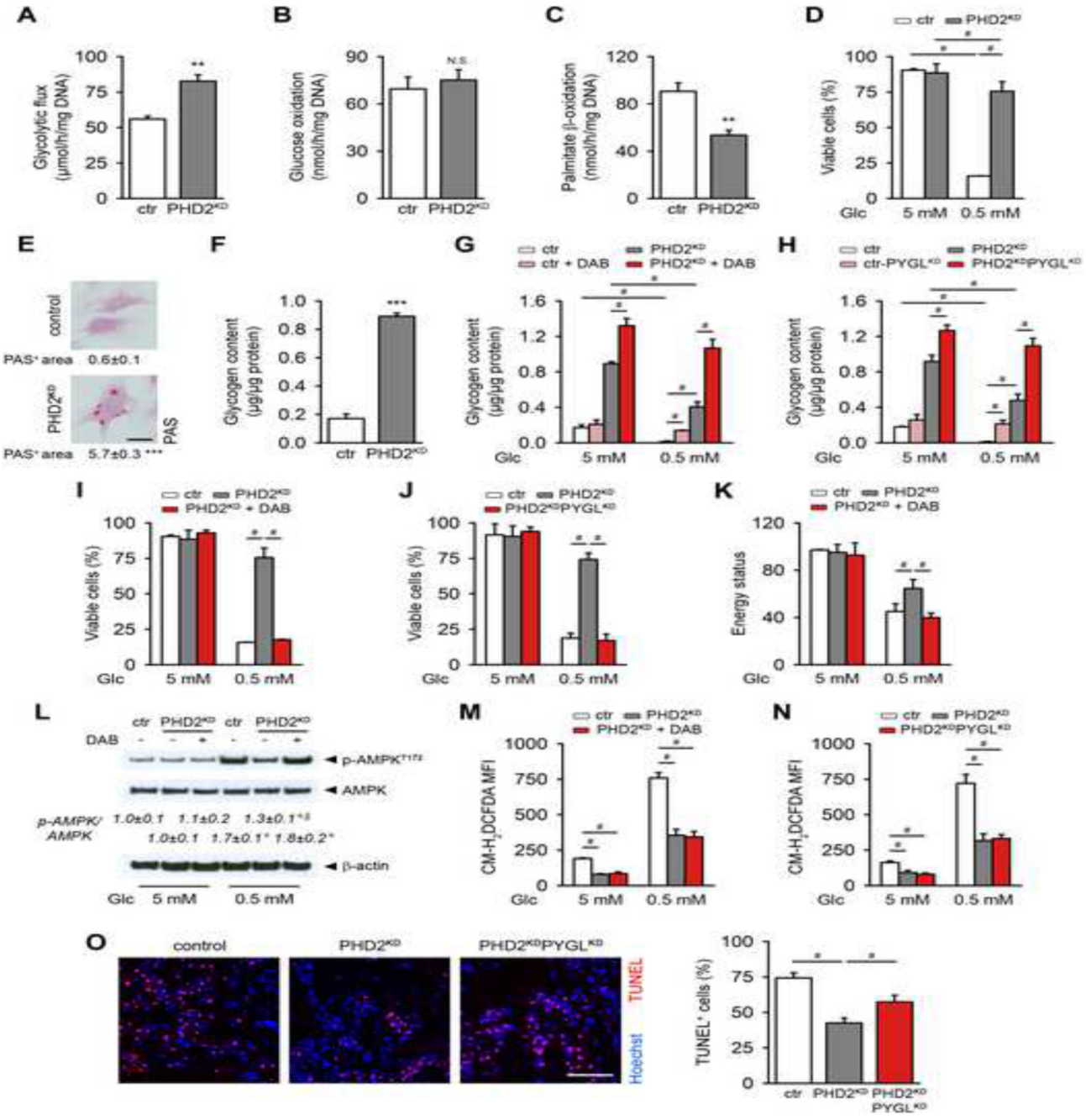

Figure 4. Glycogen Storage Contributes to PHD2^{KD} Cell Survival by Supplying Energy

(A) Glycolytic flux of cultured control (ctr) and PHD2^{KD} mPDC (n=9).

(B) Glucose oxidation rate (N.S. is not significant, n=9).

(C) Palmitate β-oxidation (n=6).

(D) Cell viability during normal (5 mM glucose) or glucose-deprived conditions (0.5 mM glucose) (n=9).

(E-F) Intracellular glycogen deposition, quantified after periodic acid-Schiff (PAS) staining (E) or determined after extraction (F) (n=9).

(G-H) Cellular glycogen content after inhibition of PYGL with DAB (G) or shRNA ($PYGL^{KD}$; H) (n=6).
(I-J) Cell viability of control, $PHD2^{KD}$ and $PHD2^{KD}$ cells after inhibition of PYGL. PYGL was inhibited in $PHD2^{KD}$ cells using DAB (I) or shRNA ($PHD2^{KD}PYGL^{KD}$; J) (n=4-6).
(K) Energy status (ratio of ATP to AMP levels) (n=3).
(L) $P\text{-}AMPK^{T172}$, AMPK and β-actin immunoblot, with quantification of $p\text{-}AMPK^{T172}$ to AMPK ratio (n=3).
(M-N) Intracellular ROS levels in control, $PHD2^{KD}$ and $PHD2^{KD}$ cells after inhibition of PYGL. PYGL was inhibited in $PHD2^{KD}$ cells using DAB (M) or shRNA ($PHD2^{KD}PYGL^{KD}$; N) (n=4-6).
(O) TUNEL immunostaining with quantification of $TUNEL^{+}$ cells in the scaffold center at day 3 after implantation (scale bar, 100 μm; n=4).
Data are means ± SEM. **p<0.01 vs. ctr, ***p<0.001 vs. ctr (Student's *t*-test), #p<0.05, °p<0.05 vs. ctr in normal culture conditions, §p<0.05 vs. ctr during glucose deprivation (ANOVA).

Europe PMC Funders Author Manuscripts

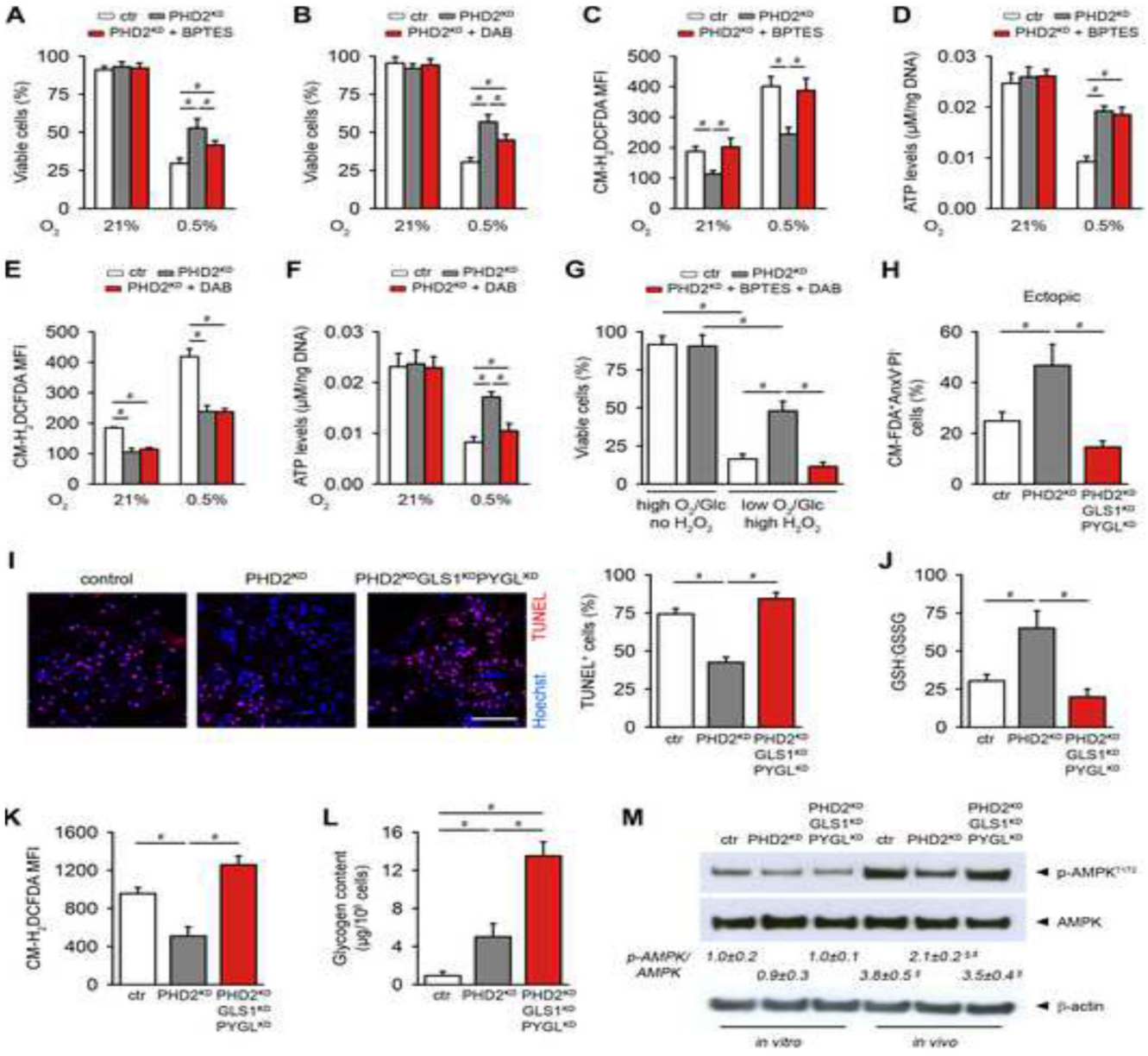

Figure 5. The Combinational Changes in Glutamine and Glycogen Metabolism Are Necessary for PHD2^{KD} Cell Viability

(A-B) Analysis of cell viability of control (ctr), PHD2^{KD} and BPTES (A) or DAB-treated (B) PHD2^{KD} cells during hypoxia (0.5% oxygen (O_2)) (n=6).

(C-F) Intracellular ROS levels (C,E) and quantification of intracellular ATP levels (D,F) in ctr, PHD2^{KD} and PHD2^{KD} cells after treatment with BPTES (C,D) or DAB (E,F) during hypoxia (n=6).

(G) Cell viability of cultured ctr cells, PHD2^{KD} cells and PHD2^{KD} cells after treatment with BPTES and DAB during normal or combined stress conditions (1% O_2), 1 mM glucose (Glc) and 12 µM H_2O_2 (high H_2O_2); n=4).

(H) Cell viability 3 days after *in vivo* ectopic implantation. Viable cells are CM-FDA^{+}AnxV^{-} PI^{-} (n=4).
(I) TUNEL immunostaining and quantification of the percentage of TUNEL^{+} cells in the center of the scaffold (scale bar, 100 μm; n=4).
(J) Ratio of GSH to GSSG in implanted CMRA-labeled ctr, PHD2^{KD} and PHD2^{KD}GLS1^{KD}PYGL^{KD} cells (n=3-4).
(K) *In vivo* intracellular ROS levels in implanted CMRA-labeled ctr, PHD2^{KD} and PHD2^{KD}GLS1^{KD}PYGL^{KD} cells (n=3-4).
(L) Glycogen content in implanted CMRA-labeled ctr, PHD2^{KD} and PHD2^{KD}GLS1^{KD}PYGL^{KD} cells (n=3-4).
(M) P-AMPK^{T172}, AMPK and β-actin immunoblot on ctr, PHD2^{KD} and PHD2^{KD}GLS1^{KD}PYGL^{KD} cells cultured *in vitro* or after *in vivo* implantation of CMRA-labeled cells, with quantification of p-AMPK^{T172} to AMPK ratio (n=3-4).
H-M: analysis at day 3 after implantation. Data are means ± SEM. $^{\#}p<0.05$, $^{\S}p<0.05$ vs ctr *in vitro*, $^{\S}p<0.05$ vs ctr *in vivo* (ANOVA).

Europe PMC Funders Author Manuscripts

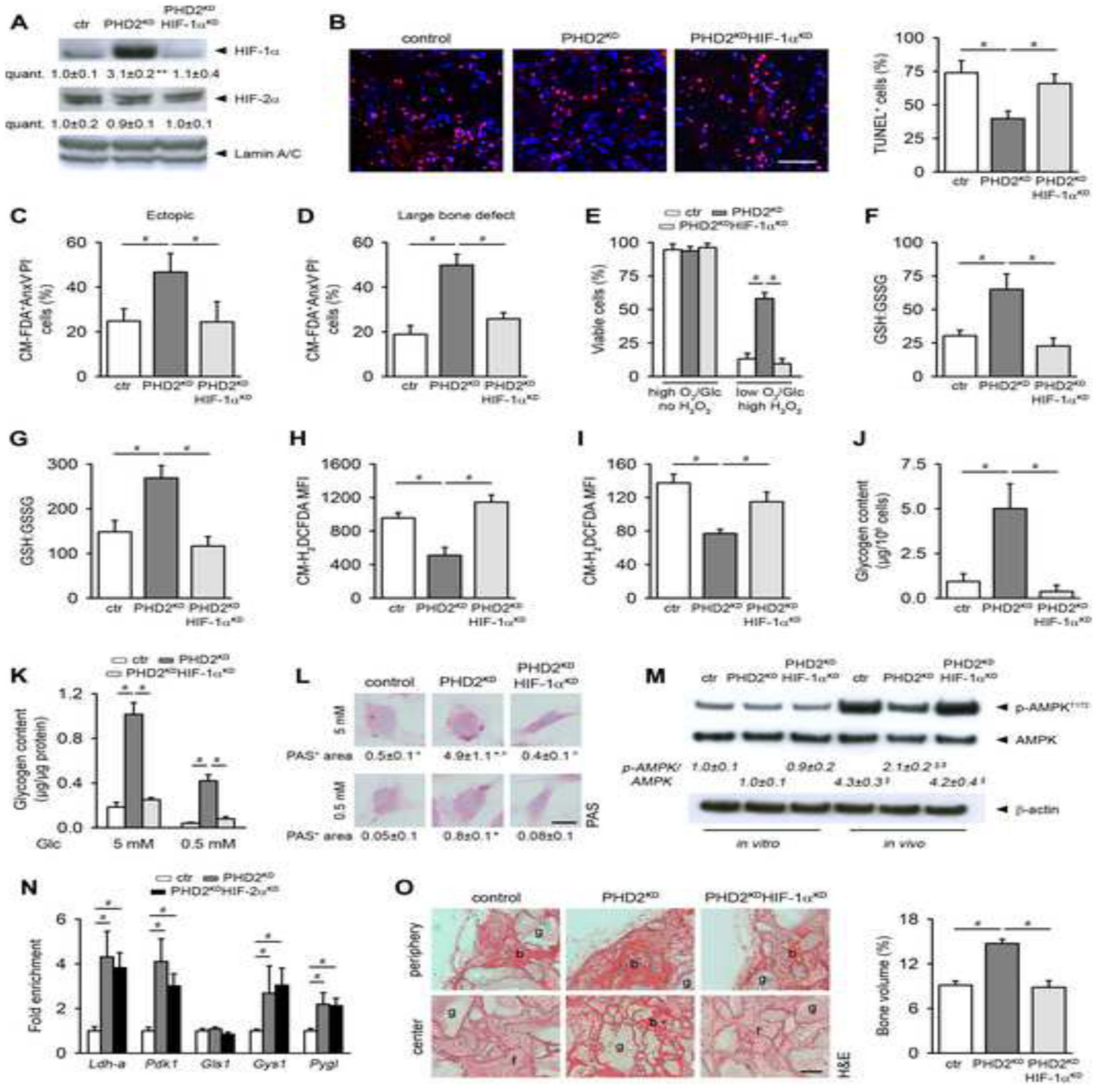

Figure 6. HIF-1α Mediates the Positive Effects on Cell Survival, Bone Regeneration and Angiogenesis in PHD2^{KD} Periosteal Cells

(A) HIF-1α, HIF-2α and Lamin A/C immunoblot of control (ctr), PHD2^{KD} and PHD2^{KD}HIF-1α^{KD} cells (n=2-3).

(B) Immunohistological quantification of TUNEL^{+} cells in the scaffold center 3 days after implantation (n=4).

(C-D) *Ex vivo* cell viability of CM-FDA labeled cells 3 days after implantation (ectopic model, C; large bone defect, D) Viable cells are CM-FDA^{+}AnxV^{-}P^{-} (n=3-4).

Europe PMC Funders Author Manuscripts

(E) Cell viability analysis on cells cultured in combined stress conditions (1% oxygen (O_2), 1 mM glucose (Glc), 12 μM H_2O_2 (high H_2O_2)). Viable cells are $AnxV^-PI^-$ (n=6).
(F-G) Ratio of GSH to GSSG in *in vivo* implanted (F; n=3-4) or *in vitro* cultured (G; n=6) ctr, $PHD2^{KD}$ and $PHD2^{KD}$HIF-$1\alpha^{KD}$ cells.
(H-I) *In vivo* intracellular ROS levels in CMRA-labeled ctr, $PHD2^{KD}$ and $PHD2^{KD}$HIF-$1\alpha^{KD}$ cells (H; n=3-4) or *in vitro* cultured cells (I; n=6).
(J) Glycogen content of implanted CMRA-labeled ctr, $PHD2^{KD}$ and $PHD2^{KD}$HIF-$1\alpha^{KD}$ cells (n=3-4).
(K-L) Intracellular glycogen deposition, determined after extraction from cells (K) or quantified after PAS staining (L) during normal culture conditions or glucose deprivation (n=4).
(M) P-$AMPK^{T172}$, AMPK and β-actin immunoblot of ctr, $PHD2^{KD}$ and $PHD2^{KD}$HIF-$1\alpha^{KD}$ cells cultured *in vitro* or after *in vivo* implantation of CMRA-labeled cells, with quantification of p-$AMPK^{T172}$ to AMPK ratio (n=3-4).
(N) Fold enrichment of HIF-1β binding to promotor regions of *Ldh-a, Pdk1, Gls1, Gys1* and *Pygl* in ctr, $PHD2^{KD}$ and $PHD2^{KD}$HIF-$2\alpha^{KD}$ cells, as determined by ChIP-qPCR (n=6).
(O) H&E staining on ectopically implanted scaffolds 8 weeks after implantation with quantification of the amount of bone formed in the total scaffold (b, bone; f, fibrous tissue; g, scaffold granule; scale bar, 500 μm; n=4).
Data are means ± SEM. *$p<0.05$ vs. ctr, **$p<0.01$ vs. ctr, °$p<0.05$ vs. ctr during glucose deprivation (Student's *t*-test), $^{\#}p<0.05$, $^{\S}p<0.05$ vs ctr *in vitro*, §$p<0.05$ vs ctr *in vivo* (ANOVA).

Europe PMC Funders Author Manuscripts

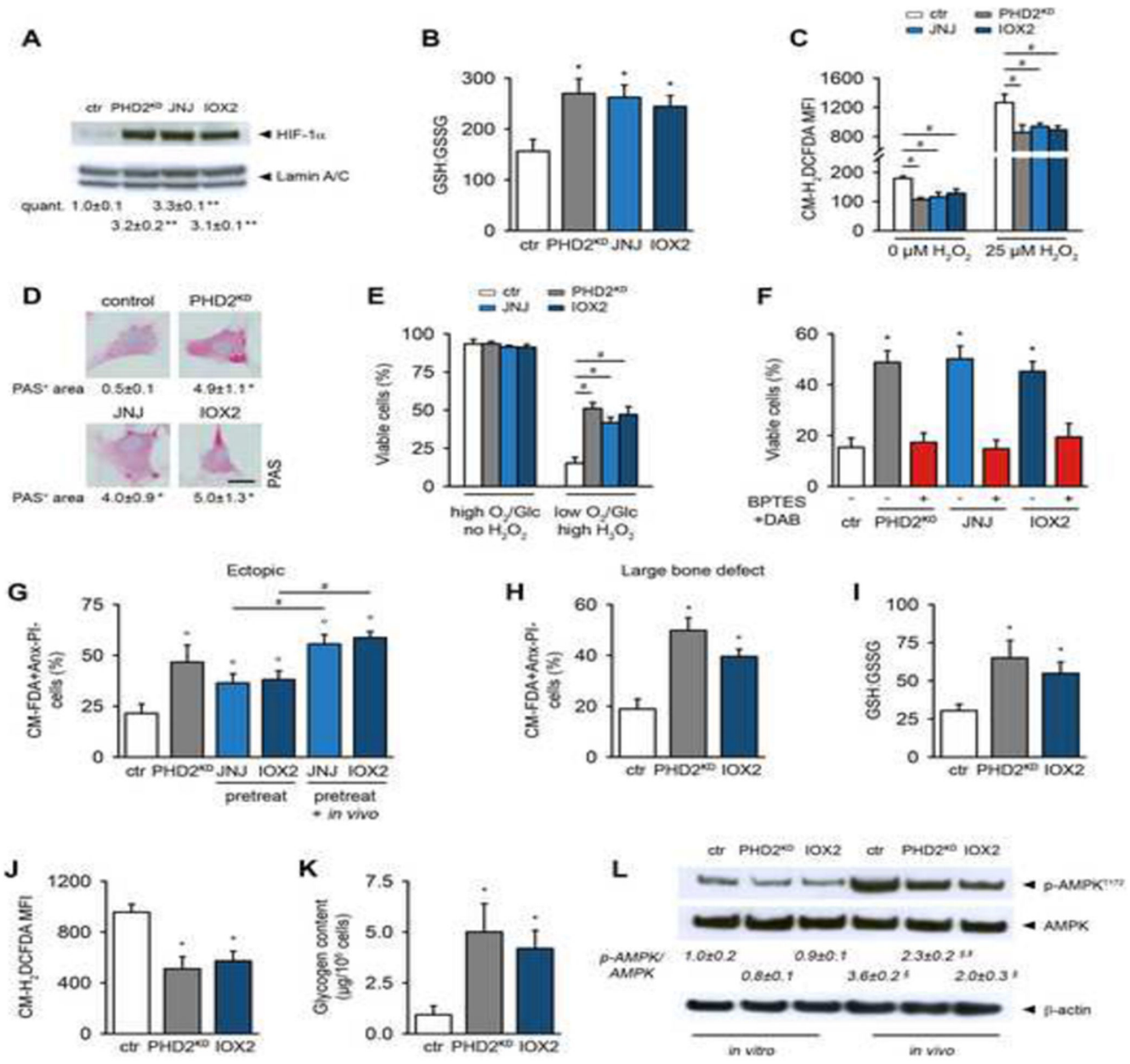

Figure 7. Pharmacological Blockade of PHDs Mimics the Effects Observed in PHD2^{KD} Cells

(A) HIF-1α and Lamin A/C immunoblot. Protein fractions were obtained 3 days after transduction of *Phd2$^{fl/fl}$* cells with Ad-Cre (PHD2^{KD}) or after 3-day treatment of wild-type cells with JNJ or IOX2 (n=3).

(B) GSH to GSSG levels in control (ctr), PHD2^{KD}, and wild-type cells treated with JNJ or IOX2 (n=6).

(C) Quantification of intracellular ROS levels in basal conditions or after treatment with 25 µM H_2O_2 (n=6).

(D) Visualization of cytoplasmic glycogen stores by PAS staining and quantification (n=4).

(E) Cell viability during normal or combined stress conditions (1% oxygen (O_2), 1mM glucose (Glc) and 12 µM H_2O_2 (high H_2O_2)) (n=6).

(F) Cell viability of cells treated with BPTES and DAB during combined stress conditions (n=6).
(G-H) *Ex vivo* cell viability 3 days after *in vivo* implantation (ectopic model, G; large bone defect, H). Compounds were also locally injected to half of the scaffolds seeded with pretreated cells (pretreat + *in vivo*, G). Viable cells are CM-FDA^{+}AnxV^{-}PI^{-} (n=4).
(I) Ratio of GSH to GSSG in *in vivo* implanted CMRA-labeled ctr, PHD2^{KD} and IOX2-treated wild-type cells (n=3-4).
(J) Flow cytometry analysis of *in vivo* total intracellular ROS levels in CMRA-labeled ctr, PHD2^{KD} and IOX2-treated wild-type cells (n=3-4).
(K) Glycogen content of implanted CMRA-labeled ctr, PHD2^{KD} and IOX2-treated wild-type cells (n=3-4).
(L) P-AMPK^{T172}, AMPK and β-actin immunoblot of ctr, PHD2^{KD} and IOX2-treated wild-type cells, cultured *in vitro* or after *in vivo* implantation of CMRA-labeled cells, with quantification of p-AMPK^{T172} to AMPK ratio (n=3-4).
Data are means ± SEM. *p<0.05 vs. ctr, **p<0.01 vs. ctr, (Student's *t*-test), °p<0.05 vs. ctr (ANOVA), #p<0.05 (ANOVA).

Europe PMC Funders Author Manuscripts